



IR vision: from chip to image/Vision IR : du composant à l'image

QWIP detectors and thermal imagers

Eric Costard^a, P. Bois^a, Alfredo De Rossi^a, A. Nedelcu^a, Olivier Cocle^b,
François-Hugues Gauthier^b, Francis Audier^b

^a *Thales Research & Technology (TRT), domaine de Corbeville, BP 56, 91404 Orsay, France*

^b *Thales optronique SA (TOSA), rue Guynemer, BP 55, 78283 Guyancourt cedex, France*

Presented by Guy Laval

Abstract

Standard GaAs/AlGaAs QWIPs (Quantum Well Infrared Photodetector) are now well established for long wave infrared (LWIR) detection. The main advantage of this technology is the duality with the technology of commercial GaAs devices. The realization of large FPAs (up to 640×480) drawing on the standard III–V technological process has already been demonstrated. The second advantage widely claimed for QWIPs is the so-called band-gap engineering, allowing the custom design of the quantum structure to fulfill the requirements of specific applications such as multispectral detection. QWIP technology has been growing up over the last ten years and now reaches an undeniable level of maturity. As with all quantum detectors, the thermal current, particularly in the LWIR range, limits the operating temperature of QWIPs. It is very crucial to achieve an operating temperature as high as possible and at least above 77 K in order to reduce volume and power consumption and to improve the reliability of the detection module. This thermal current offset has three detrimental effects: noise increase, storage capacitor saturation and high sensitivity of FPAs to fluctuations in operating temperature. For LWIR FPAs, large cryocoolers are required, which means volume and power consumption unsuitable for handheld systems. The understanding of detection mechanisms has led us to design and realize high performance ‘standard’ QWIPs working near 77 K. Furthermore, a new in situ skimmed architecture accommodating this offset has already been demonstrated. In this paper we summarize the contribution of THALES Research & Technology to this progress. We present the current status of QWIPs in France, including the latest performances achieved with both standard and skimmed architectures. We illustrate the potential of our QWIPs through features of Thales Optronique’s products for third thermal imager generation. **To cite this article:** *E. Costard et al., C. R. Physique 4 (2003).*

© 2003 Académie des sciences. Published by Elsevier SAS. All rights reserved.

Résumé

Détecteurs à multipuits quantiques et caméras infrarouge. 15 ans après la première démonstration de laboratoire de l’absorption infrarouge dans une structure à multipuits quantiques (QWIP) par B. Levine, ce type de détecteur est désormais intégré dans des systèmes opérationnels. Durant la dernière décennie, THALES Research & Technology a concentré ses efforts dans l’optimisation des performances de détecteurs élémentaires, en particulier pour des températures d’exploitation autour de celle de l’azote liquide. Le développement d’un modèle auto consistant tenant compte de l’ensemble des paramètres physiques et électrooptiques d’un détecteur élémentaire, nous a permis de fabriquer des QWIPs couvrant l’intégralité de la bande spectrale 4–18 μm et dont les performances représentent l’état de l’art. Après une première collaboration en 1997 avec Sofradir pour la réalisation d’un démonstrateur au format modeste de 144×192 , nous développons et produisons aujourd’hui des plans focaux QWIPs aux formats 384×288 et 640×512 . Dans cet article nous présentons les premiers résultats obtenus avec une matrice 640×512 hybridée sur le circuit ISC9803 d’Indigosystem. Les sensibilités accessibles avec notre structure QWIP classique obtenues à 75 K sont suffisantes pour un grand nombre de besoins opérationnels. Nous introduisons ici notre nouveau concept d’ébasage intégré dans le pixel qui permettra de relâcher cette contrainte de température de fonctionnement des détecteurs QWIPs. **Pour citer cet article :** *E. Costard et al., C. R. Physique 4 (2003).*

© 2003 Académie des sciences. Published by Elsevier SAS. All rights reserved.

Keywords: Focal plane arrays; QWIP; Skimming function; Long wavelength infrared range

Mots-clés : Détecteurs matriciels ; Détecteurs multipuits quantiques ; Ébasage ; Infrarouge lointain

1. Introduction

15 years after the laboratory demonstration of intersubband IR absorption by Levine [1] in QWIP structures, this type of detector is today ready to be integrated in operational systems. For the last decade THALES Research & Technology has made a great effort in optimizing the performance of elementary detectors, in particular for operating temperatures around that of liquid nitrogen. Through the development of a selfconsistent model that takes into account all the physical and electrooptical parameters of a pixel, we have been able to fabricate QWIPs in the 4–18 μm band whose performance represents the state of the art. Following a first collaboration in 1997 with Sofradir [2] on a demonstrator of a modest format of 144×192 , we now together develop QWIP FPAs having formats of 384×288 and 640×512 . In this article we present the first results obtained on a FPA 640×512 , employing a ROIC from Indigo. With the help of these results we illustrate the sensitivity degradation as a function of increasing temperature of operation. The NETDs accessible with our classical QWIP up to 75 K are sufficient for the operational requirements. However, only our in situ skimming concept in the active layer makes it possible to relax this operational temperature restriction. Here we present our progress in developing FPAs that incorporate the skimming functionality.

2. Modeling and experimental results

A global electrooptic model has proven essential to optimizing the intrinsic QWIP performances. Fig. 1 presents the full list of parameters involved in the evaluations. In order to calculate the electron transport we take into account the optical coupling (different coupling schemes were studied but for sake of simplicity, we consider in this paper diffraction gratings only). We recall that the active layer is located in the near field zone, and we use a modal approach for the modeling. To be complete, we take also into account, for the optimization process dedicated to a specific application, operational constraints such as operating temperature, bias voltage, optical flux and maximal allowed integration time.

To verify the agreement between the optical coupling model and experiments we have fabricated pixels having gratings of different pitch on one heterostructure composed of 40 wells designed for a photoresponse centered around 8.6 μm . We show the spectral responses in Fig. 2 with finely spaced grating periods from 2.5–3 μm .

The photocurrent generated by the detectors will be proportional to the integral of those spectral responses. In Fig. 3 we plot the evolution of that integral as measured and compare it to the values given by the model. The comparison shows the good agreement between the model and the experiment. Furthermore, it is striking that the integral varies slightly with the grating period from 2.5–2.7 μm . The grating technology has for a long time been considered a major drawback, but it is no longer an obstacle and can be turn out to be a powerful tool for making smart detectors.

Thus the optical coupling model makes it possible to define precisely the grating parameters with the goal of optimal absorption in the heterostructure. However, we go futher in our optical modeling approach. In fact, as far as large arrays are concerned, the pitch should be reduced in order to keep the focal plane to a reasonable size. We then consider finite size effects and developed a new modeling which we shall briefly introduce later.

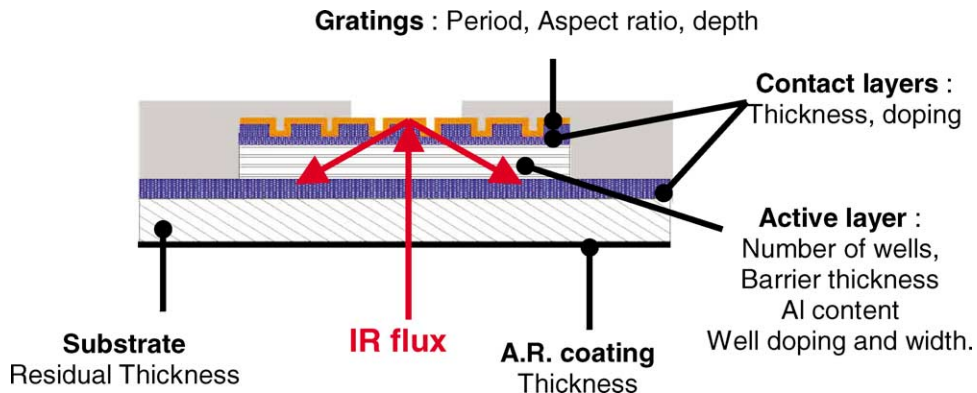


Fig. 1. Parameters taken into account for global modeling.

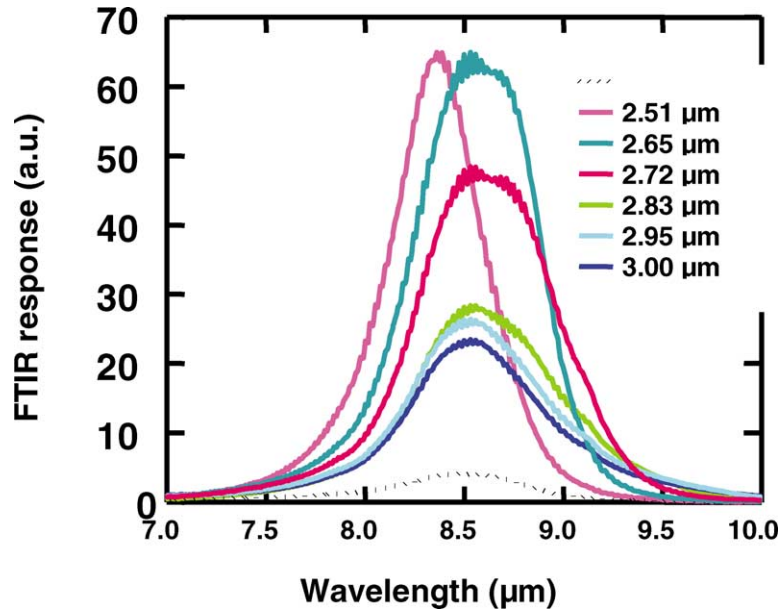


Fig. 2. Variation of the spectral response with the grating period for a QWIP designed at 9 μm.

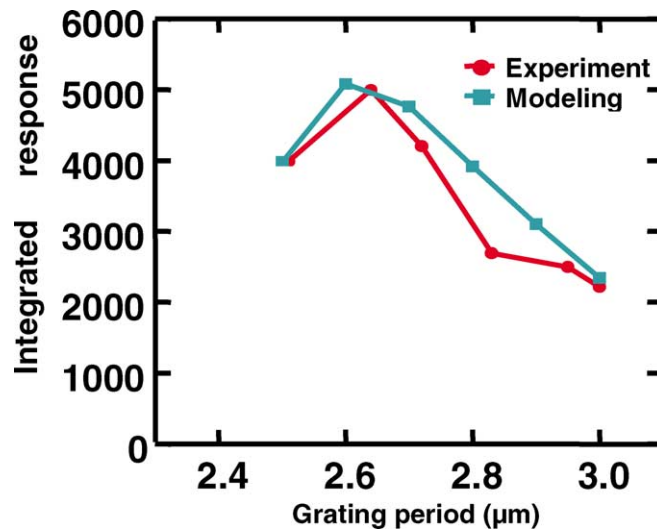


Fig. 3. Evolution of the integrated spectral response with the grating period, and comparison with modeling.

The modal expansion method (MEM) is generally used to design gratings and it consists in matching the modes in the grating grooves with the Rayleigh expansion [3]. This method is effective in determining the coupling efficiency, as far as the grating can be assumed of infinite extension. As shown in the following, the pixel pitch is shorter than 30 μm (i.e., less than 12 grating periods). Therefore, we have focused on finite size effects. Proper modeling is done through a finite element code, with the specific advantage of representing complex geometries through adaptive meshing. Unphysical reflections of the outgoing field are eliminated thanks to the Perfectly Matched Layer (PML) [4].

The intensity of the electric field polarized along the growth direction ($|E_y|$) is shown in Fig. 4. At the grating resonance wavelength (=maximum grating coupling) it is apparent that a surface wave is excited. This wave decays exponentially with the depth. It is therefore interesting to place the MQW close to the grating. This approach allows us to take into account finite pixel size effects and, indeed, provides an explanation of the observed experimental dependence of the responsivity on the pixel size (Fig. 5).

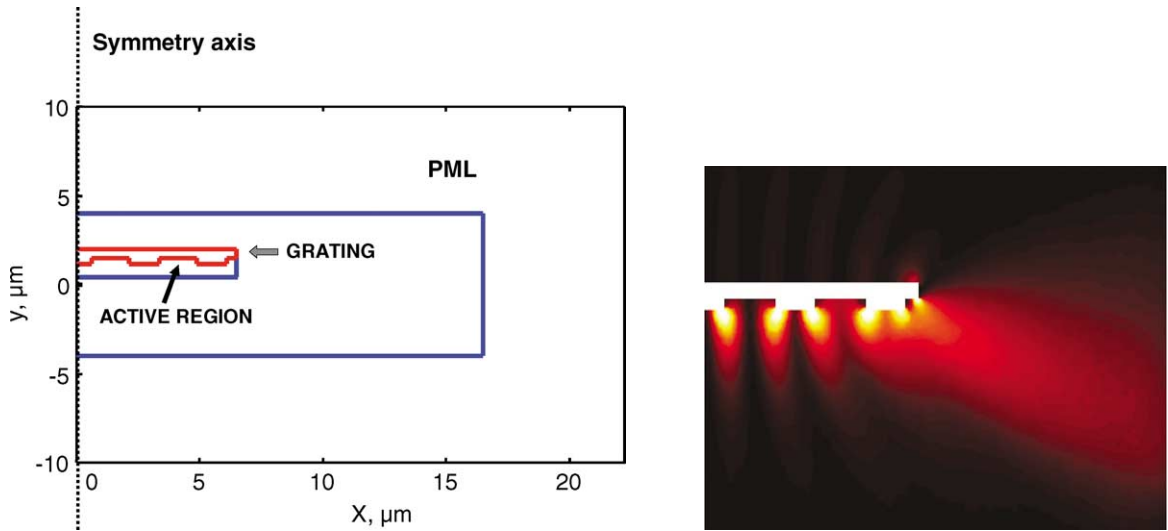


Fig. 4. Left: finite size pixel; right: 'y' polarized field $|E_y|$ at resonance.

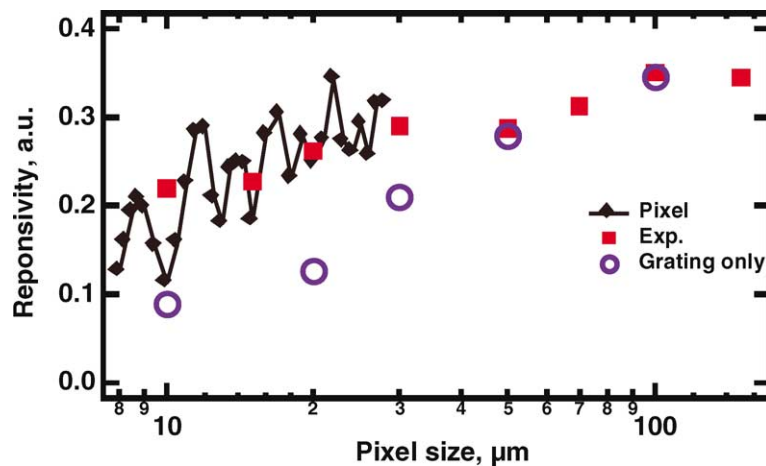


Fig. 5. Responsivity versus Pixel size.

Experiments using detectors with varying pixel size (squares) show that responsivity does not decrease as fast as expected considering a finite size grating (circles). The correct trend is predicted when including into the model the pixel geometry, thus allowing additional scattering from pixel walls (line with symbols). Oscillations are due to internal resonance.

Modeling electronic transport is also imperative for the quantum well design in order to take into account the operational requirements like bias voltage and offset current. In order to illustrate the relevance of our global model we report here an experimental fact that only this calculation could predict. In Fig. 6 we show the spectral responses of a typical QWIP structure for two different operating temperatures and the same experimental conditions. The 50 K response of that detector (in the BLIP regime) is slightly lower than that obtained at 80 K (thermionic regime).

The electric field inside the heterostructure is not homogeneous, and its distribution depends strongly on the electronic injection at the contact and also on the emission phenomena at each well; so the calculated electric field distributions in the heterostructure for both temperatures are different (Fig. 7). In the BLIP regime the distribution is dominated by the grating effect (non-uniform electromagnetic field distribution along the heterostructure) while in the thermionic regime the thermal emission remains nearly constant at each well.

From the electric field distribution electrical characteristics can be deduced. Fig. 8 presents the evolution of the response with bias voltage for both temperatures. In agreement with the experimental finding, at low bias the expected response in the BLIP regime is lower than in the thermal regime.

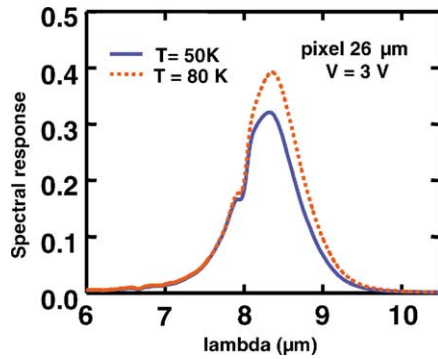


Fig. 6. Comparison of spectral responses in both blip and thermionic regimes.

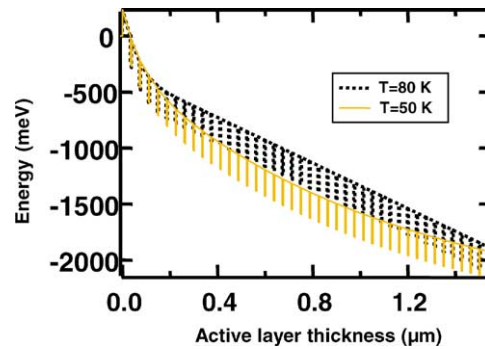


Fig. 7. Calculated electric field distributions for a 40 wells QWIP at 50 K and 80 K.

Actively exploiting this model, we have optimized and fabricated QWIP detectors in all the LWIR and MWIR bands. We show the spectral responses together with the peak detectivities for an $f/1.6$ aperture and a background temperature of 300 K in Fig. 9. The combinations of detectivity and operating temperature reported here represent the state of the art of QWIPs.

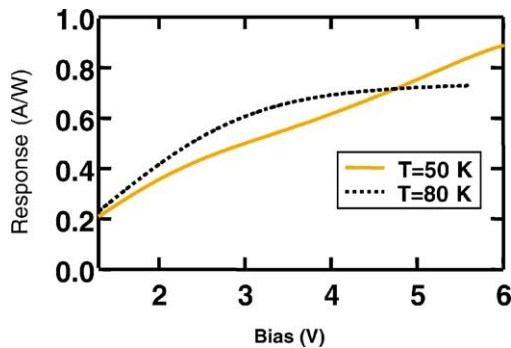


Fig. 8. Calculated response versus bias voltage in BLIP and thermionic regimes.

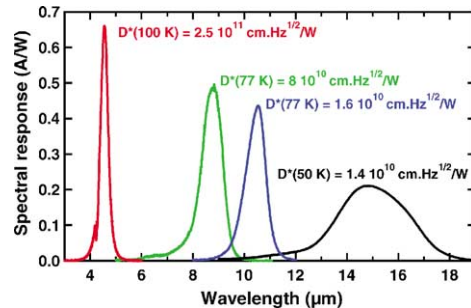


Fig. 9. Different QWIP spectral responses and detectivities obtained at Thales.

3. QWIP FPA development in France

Combining their respective skills, Thales and Sofradir develop QWIP focal plane arrays for imaging at 9 μm . Three programs are pursued:

- 384 \times 288 classical QWIP (pitch 28 μm , RM5 cryocooler from Cryotechnology);
- 640 \times 512 classical QWIP with a ISC9803 ROIC from Indigo System (pitch 25 μm , 1 W cryocooler);
- 384 \times 288 in pixel skimming mode QWIP (pitch 28 μm , RM2 cryocooler from Cryotechnology).

Thales realizes the design and fabrication of the QWIP arrays, and the hybridization and integration in IDDCA are integrator's task (Sofradir,...). The QWIP processing is perfectly compatible with all the hybridization procedures. The SEM picture (Fig. 10) shows a detail of a classical 28 μm pitch array before hybridization. A systematic use of plasma etching makes possible very high filling factors ($>85\%$) and a strict control of dimensions preserving the intrinsic epitaxial uniformity.

The fabrication yields obtained today on a GaAs wafer are above 60%, and the operating yield per array is better than 99.9% even for the full TV format FPAs. While hybridization is completely mastered by integrators, we still had to develop and stabilize the GaAs substrate thinning step after hybridization. This is now behind us, and the technology is compatible with large volume production. The SEM pictures (Fig. 11) show in cross section a 384 \times 288 FPA before and after this thinning step.

The QWIP FPAs are then mounted in cryostat by integrators (Fig. 12). All these packaging steps are also compatible with the production techniques already employed for other cooled detectors.

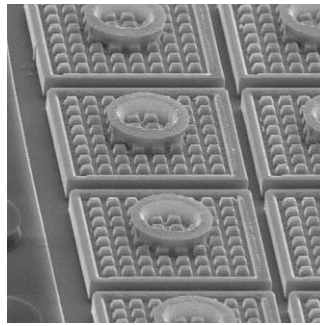


Fig. 10. Detail of a 384×288 classical QWIP array before hybridization.

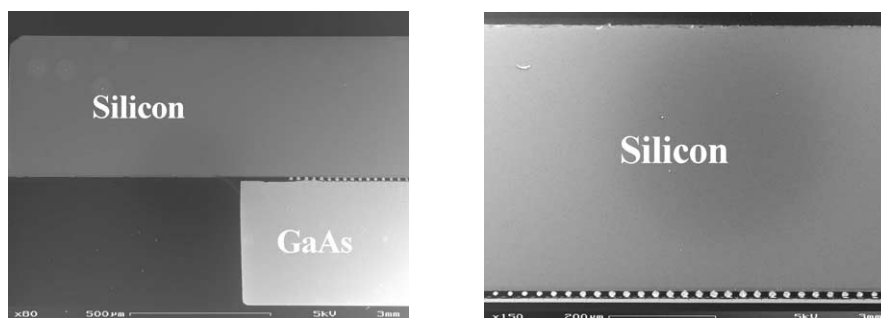


Fig. 11. Right: SEM cross section before; and left: after GaAs substrate removal.

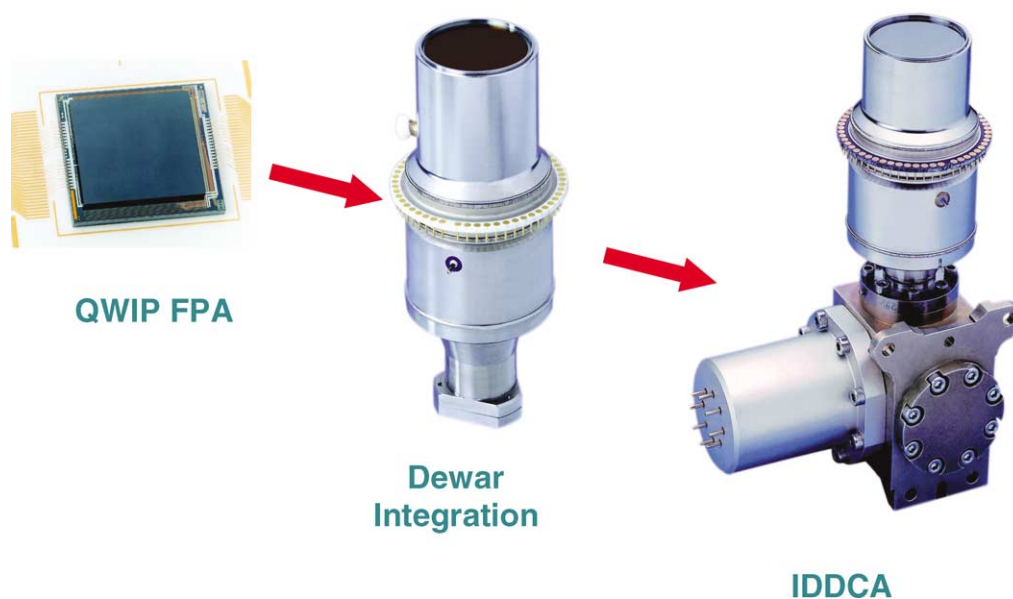


Fig. 12. Main steps for QWIP FPA integration at Sofradir.

The first results obtained with the 640×512 FPA were obtained in an EmeraldTM demonstrator designed by the French company CEDIP. CEDIP designed and fabricated the $f/2$ optical system as well the proximity electronics and the body of this camera. The spectral response is centered on $8.5 \mu\text{m}$ (Fig. 13).

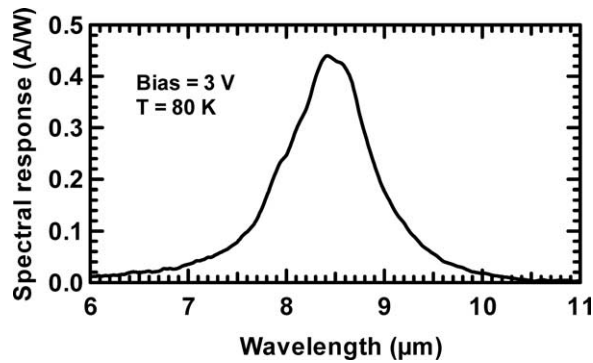


Fig. 13. Typical spectral response of QWIP FPAs at 80 K and for a 3 V bias voltage.

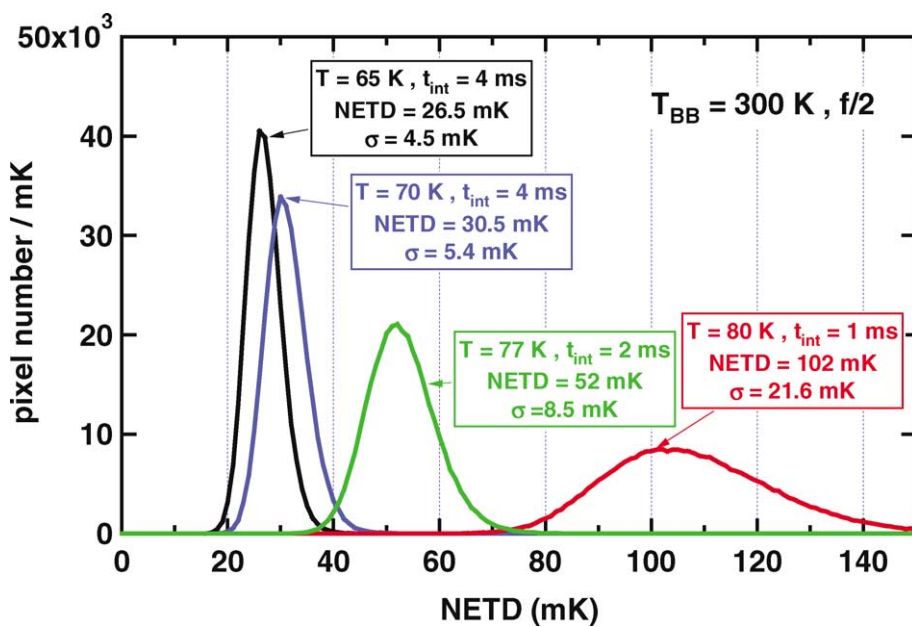


Fig. 14. NETD histograms for different operating temperatures of the 640×512 QWIP FPA.

In Fig. 14 we show the NETD histograms for different operating temperatures. Above 77 K the increase of the thermally activated dark current imply a reduction in allowable integration time. The direct consequence of this is a sensibility decrease of the component. Nevertheless, it must be noted that the performances reached for $T < 77$ K are sufficient to comply with the requirements of the new camera generation. The histograms presented here are not corrected for the field of view effect induced by the cold shield at $f/2$.

In order to circumvent this operating temperature limitation we have introduced the new concept of in situ skimming in the active layer [5], which we briefly recall in the next section.

4. In situ skimming principle

The basic idea is to benefit from the excellent reproducibility and uniformity of QWIPs, by growing a stack of two QWIP layers. The whole structure is a simple impedance bridge (see Fig. 15). The top (t) QWIP stack is the detecting stage, whereas the bottom (b) stack acts as the reference arm of the bridge. The two bias voltages V_s and V_{ref} are applied on the extreme contacts, and the signal is extracted by an intermediate contact hybridized by an indium bump to the silicon ROIC.

This functionality can easily be implemented in the pixel itself by using the architecture of our two color detectors [6].

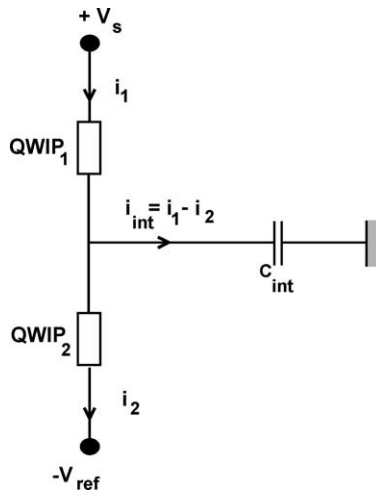


Fig. 15. Sketch of the integrated skimming architecture.

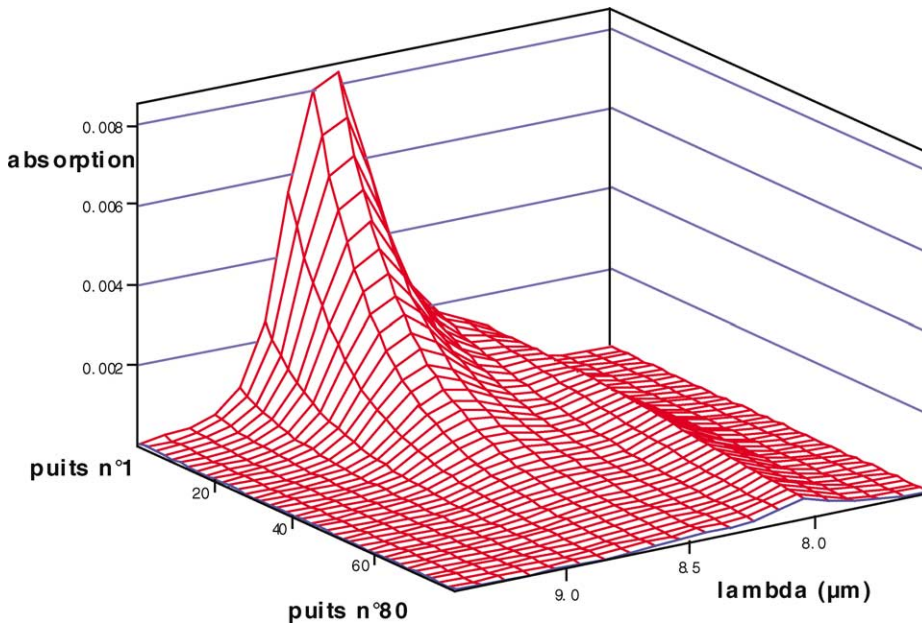


Fig. 16. Calculated spectral absorption per well for an 80 well stack coupled with an optimal grating.

For each bottom or top stage, the total current is given by: $i_{b,t} = i_{b,t}^{dark} + i_{b,t}^{opt} = i_{b,t}^{dark} + i_{b,t}^{bkg} + i_{b,t}^{sig}$, where the superscript ‘bkg’ is used for the continuous optical part, and ‘sig’ for the ‘useful’ signal. Let us assume two identical QWIP stacks, with the same $I-V$ curve. For the same biases $V_s = V_{ref}$, the difference between the two currents eliminates the dark current and the operating temperature problems. The integrated signal i^{int} becomes: $i^{int} = i_t - i_b = i_t^{opt} - i_b^{opt}$.

Even if the two QWIP stacks are identical, it is possible to detect a non-zero signal. The two active layers are identical, but thanks to the gratings required for coupling the infrared light to QWIPs, the responsivities of the two stacks are different. The same grating is used for the two stacks, but the near field diffraction coupling efficiency of the grating depends strongly on the distance from the grating. In Fig. 16 the calculated absorption per well for an 80 well structure is shown. The efficiency of the grating is much higher for the first 40 wells (detector stage of the skimming pixel) than for the last 40 wells (reference stage), so the resulting integrated photocurrent will not be too degraded.

In this operating mode, the integration time can be extended up to the video frame time, enhancing simultaneously the NETD and the imager dynamics.

5. In situ skimming QWIP focal plane performances modeling

In a development of IR FPAs, the readout integrated circuit is the second major part next to the infrared transducer array. Readout circuits are designed to support a good interface between detecting elements and the following signal processing stage.

There are three detector readout approaches: voltage sensing, current sensing and charge sensing. The appropriate approach is determined by the detector electrical parameters. To meet high transfer efficiency of the detector electrical signal to the readout circuit, high impedance detectors are coupled to low-input impedance current sensing circuits, whereas low impedance detectors are coupled to high-input impedance voltage sensing circuits.

The most common readout circuit topologies are based on one of the following schemes: Direct Injection (DI), Buffered Direct Injection (BDI), Source Follower per Detector (SFD), Gate Modulation Input (GMI) and Capacitive Trans-Impedance Amplifier (CTIA).

The choice of a readout scheme is dependent on the application and must take into consideration unit cell size, signal-to-noise ratio, linearity, dynamic range and power dissipation.

In the LWIR applications, high background charges combined with high dark current, which introduce additional shot noise and increase the dynamic range requirement to meet high sensitivities, have to be accommodated by a finite integration capacitance that can saturate rapidly. This constraint is valid for MCT detector as well as for QWIP detector which, despite their relatively high impedance, exhibits a high dark current resulting from the high bias voltage operation.

To alleviate this problem, the dark current and partial background suppression, prior the integration, can be used to improve detection sensitivity, dynamic range and application range. To date, the background suppression was performed by the readout circuit itself, implying some additional electronics operating in the charge domain, which cannot solve the analyzed problem, or using current mode before integration. Among the multiple drawbacks of these readout circuit solutions we quote the reduction of the available silicon area for the signal storage and the degradation of the focal plane offset uniformity.

In the skimming QWIP architecture, since current subtraction is performed in the transducer itself, no extra subtractive circuit is required, preserving almost all the injection cell area available for charge integration.

The direct injection circuit is one of the simplest structure scheme. It can be designed with only 3–5 transistors per unit cell. It allows good detector bias control during the integration time and the cell dissipates no active power as in the case for most other more complex circuit architectures like BDI and CTIA. This makes it suitable for high density IR FPAs with provision for large charge handling capacity.

5.1. Integrated signal using a basic Direct Injection circuit

The QWIP Direct Injection architecture is illustrated by Fig. 17. The operation of the cell is as follows:

First the integration capacitor is reset to a reference level by pulsing the reset transistor. The common gate transistor, biased to a voltage close to its threshold voltage, fixes the potential of the common contact of the detecting and subtracting QWIP layers and presents a low input impedance to the detector.

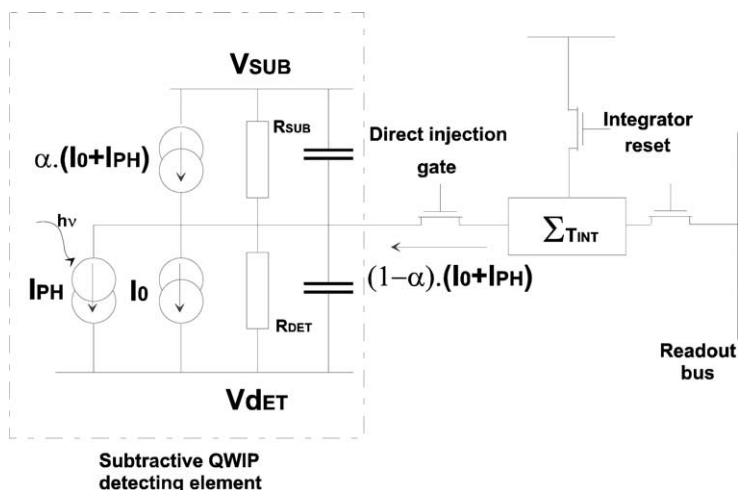


Fig. 17. Schematic of QWIP detecting element readout using a basic Direct Injection circuit.

Assuming a quasi nonphoto-sensitive subtracting layer (at least in the wavelength range of interest), the residual current is the sum of the photo-current and dark current flowing through the detecting layer, diminished by the polarization current of the subtracting layer: $(I_{01} + I_{ph}) - I_{02}$.

Let assume that the subtracted current is proportional to the current flowing through the detecting layer, the residual current can be expressed as: $(I_0 + I_{ph})(1 - \alpha)$ with $0 \leq \alpha < 1$.

For very low residual currents (α close to 1), the injection efficiency, defined as the ratio of the integrated current to the residual current, may become very low since the detector impedance decrease as the subtraction level, controlled by the subtracting layer polarization, increases. Thus the injected and the integrated current is modeled by: $\eta_{inj}(I_0 + I_{ph})(1 - \alpha)$.

Note that the detection efficiency may be quasi-total, regardless of the subtracting level, using a high gain feedback amplifier to decrease the input impedance of the injection transistor. Of course this has to be done at the expense of the input cell dynamic.

5.2. Sensitivity evaluation

Temporal noise consists of fundamental photon shot noise that varies as the square root of the number of integrated photo-electrons, detector noise and additional noise introduced by the readout electronics. In high background applications and for a detector having high dark currents, the readout electronics noise is rapidly insignificant and may be, in a first approximation, neglected.

$$v_n = \frac{1}{C_{int}} \sqrt{2q\eta_{inj}(I_0 + I_{ph})(G_{pc1} + \alpha G_{pc2})T_{int}},$$

where

- I_0 = QWIP dark current,
- I_{ph} = QWIP photo current,
- G_{pc1}, G_{pc2} = photo conduction gain of the two QWIP layers,
- η_{inj} = injection efficiency,
- T_{int} = integration time,
- q = electronic charge,
- C_{int} = integration capacity.

The integration time leading to an integrated charge corresponding to only a part (K) of the integrator charge handling capacity ' Q_{max} ' corresponds to

$$T_{int} = K \frac{Q_{max}}{\eta_{inj}(I_0 + I_{ph})(1 - \alpha)},$$

where $0 \leq \alpha < 1$ is the current subtraction level, and $0 \leq K < 1$.

The Noise Equivalent Temperature Difference (NETD), of the focal plane representing the temperature change, for incident radiation, that gives an output signal equal to the rms noise level, is defined as: $NETD = v_n(\Delta T / \Delta V_s)$, where ΔV_s is the signal measured at a background temperature T and for the temperature difference ΔT .

$$\Delta V_s = T_{int} f(T, \Delta T, \Re_\lambda), \text{ where } \Re_\lambda = \text{the QWIP responsivity (A/W)}.$$

It then can be shown that:

$$NETD = \frac{2\eta_{inj}(I_0 + I_{ph})\sqrt{qG_{pc}(1 - \alpha^2)}}{C_{int}\sqrt{Q_{max}}f(T, \Delta T, \Re_\lambda)}$$

can be expressed as: $NETD = NETD_{\alpha=0}\sqrt{1 - \alpha^2}$.

5.3. Calculation results

To evaluate the skimming QWIP detector performances, some calculations have been carried out according to the following assumptions:

- Detecting element area: $30 \mu\text{m} \times 30 \mu\text{m}$,
- Peak responsivity: 0.5 A/W ($\lambda_{pic} = 8.8 \mu\text{m}$),
- Dark current at 77 K: 1 nA ,

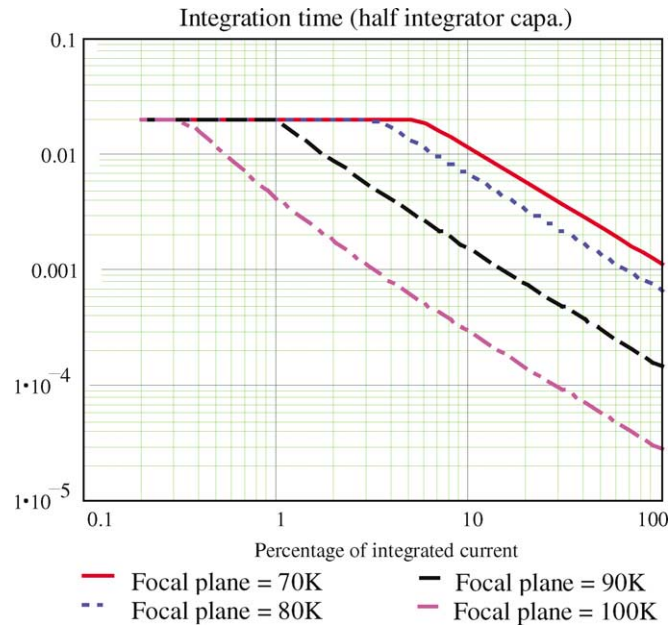


Fig. 18. Integration duration versus the percentage of detector current injected. The integration time is limited either by a 3 pC integrated charge or by 20 ms frame rate.

- Gain of photo-conduction: 0.4,
- Fill factor: 92%,
- Background temperature: 290 K,
- Total integrator charge handling capacity: 6 pC,
- Maximum integrated charge: 3 pC ($K = 0.5$),
- Direct injection.

Fig. 18 shows the optimized integration time for several focal plane operating temperatures (65 K to 100 K). The constraints applied to the calculation are:

- maximum integrated charge limited to half of the integrator capacity (3 pC). This limitation fixes the quasi proportionality existing between the allowed integration duration and the subtraction level;
- maximum integration time limited to 20 ms.

Fig. 19 shows the sensitivity variation versus the subtraction level for focal plane operating temperatures ranges between 65 K and 100 K:

- A remarkable reduction of the NETD, proportional to the subtraction factor $\sqrt{1 - \alpha^2}$, can be observed for any operating temperature. At a practical or typical subtraction level, sensitivities as high as those obtained at 65 K are achievable for operating temperature approaching 90 K.
- At very high subtraction levels, performance improvement is limited by the maximum available integration time.
- At a high operating temperature and a high subtraction level, performance degradation is observed. This results mainly from the noise associated with the high dark current derived before the integration, and is amplified by a signal attenuation due to an increase in the injection inefficiency. At this operating point, the loss in signal-to-noise ratio cannot be compensated by the limited integration time.

6. Latest results on in situ skimming FPA

The sample quantum structure consists of two stacks of standard GaAs (5 nm)/Al_{0.22}Ga_{0.78}As (35 nm) multi-quantum well layers, clad by two n⁺ GaAs contact layers, and separated by an intermediate n⁺ GaAs contact layer. Following our bispectral

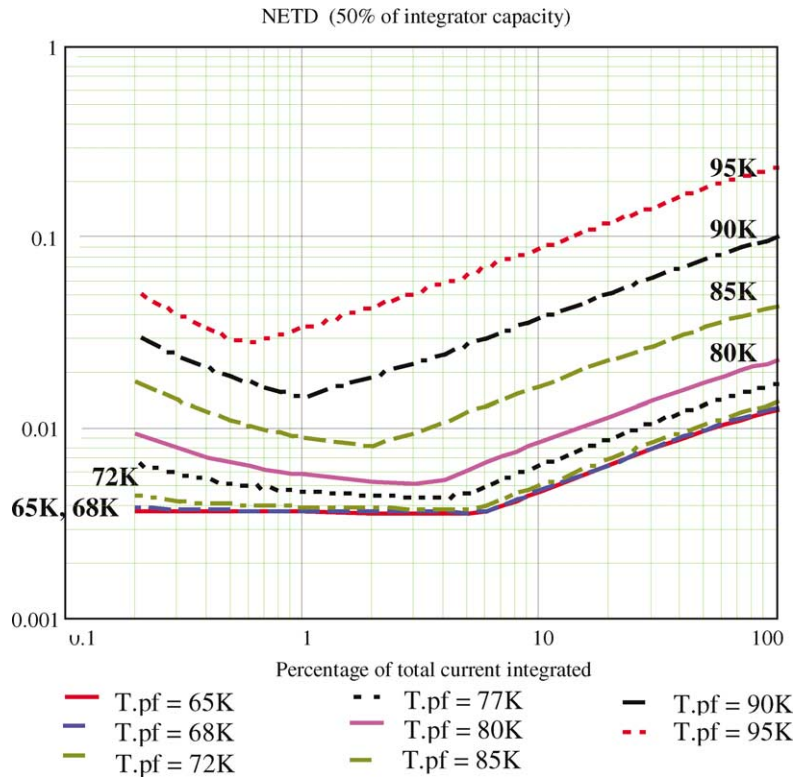


Fig. 19. NETD evolution versus the percentage of detector current injected. The NETD reduction is limited by the maximum allowed integration time.

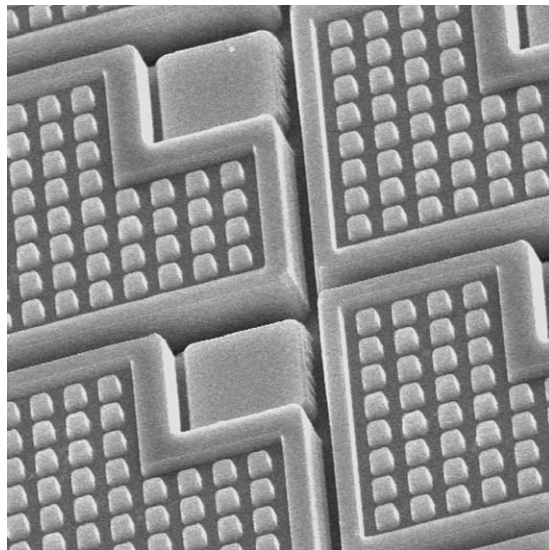


Fig. 20. SEM picture of a 3-contact pixel before the interconnection step (pitch = 28 μm, filling factor = 83%, etched height = 5 μm).

process, gratings are fabricated on the top of the pixels. The pixels are defined by *i*-line photolithography and dry etching as for classical QWIP. Fig. 20 is a detail of the FPAs (format 384 × 288, pitch 28 μm) that Thales and Sofradir are currently developing.

We present in Fig. 21, the spectral response of our first in situ skimming FPA in three operating conditions at 80 K. The spectral responses of each independent stack are measured with only one bias voltage applied V_s or $-V_{ref}$ (near 2 V), leading

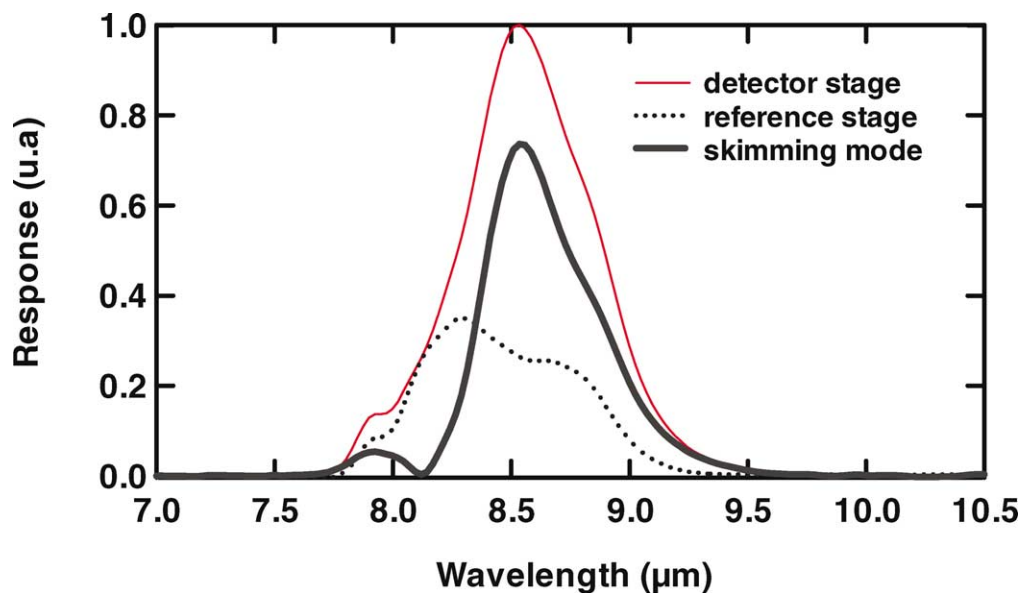


Fig. 21. Spectral responses for each stage of the shimming pixel and in skimming mode.

to the same dark current. Then, by applying simultaneously the two bias voltages, the continuous part of the current can be decreased from 2 nA to 0.2 nA. The spectral response of the resulting detector exhibits a degradation of 40% in the responsivity only.

However, the degradation of both responsivity and noise is largely compensated by the potential increase of the integration time. By using the detector stage alone ($f/3$ and $T_{bb} = 300$ K) the measured NETD at 80 K was 120 mK with an integration time limited to 1 ms. In the skimming mode the integration time can be increased up to 10 ms leading to a NETD of 70 mK.

These results were obtained in our first attempt with in situ skimming QWIP FPAs. We add also that the pixel operability was as high as 99% on this first attempt.

7. QWIP thermal imager

Thales is now offering classical QWIP focal plane in 1/4 TV format Architecture and performances of this thermal imager named 'Catherine QWIP' are now described (Fig. 22).

In close cooperation with Thales Research and Technology team Thales Optronique has developed a very compact thermal imager that benefits from the last QWIP development and also from integrated electronics.

Thanks to the stability of the QWIP transfer function the non-uniformity correction is limited to a two points calibration in factory and a one point calibration during initialization phase.

The architecture based on powerful FPGA and DSP keeps a great capacity to integrate further development of complex algorithm.

Two versions (Fig. 23) are today available:

- Basic version NFOV: 4°, WFOV: 10°;
- Basic version NFOV: 3°, WFOV: 9°.

7.1. Main characteristics (basic version)

- Operating spectral bandwidth: 8–12 μm
- NETD < 65 mK ($F/3$)
- Weight: 2.5 kg/Size: 217 × 172 × 100 (mm)

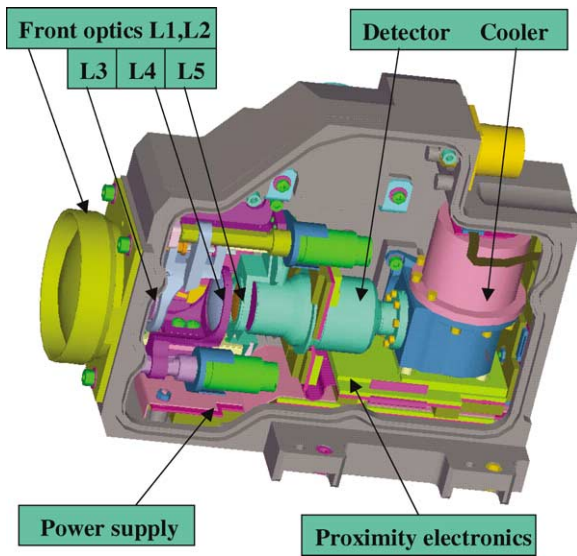


Fig. 22. Catherine QWIP architecture.



Fig. 23. Left: Catherine QWIP in 4° FOV Version; and right: 3° FOV Version.

8. Conclusion

The operating temperature improvement allowed by the new QWIP transducer architecture will introduce greater flexibility for the Dewar and cryogenic cooling system. The newly accessible performances will reduce (even cancel) the traditional operating temperature handicap of the QWIP GaAs detectors, while preserving the exceptional qualities of their electro-optical performances and other large focal plane industrial feasibility aspects. However, the performance of classical QWIP FPAs obtained at 75 K already meet the requirements of the new generation of imagers, and THALES Optronique has based its today strategy on very compact thermal imagers in order to allow the largest panel of applications for hand held and vehicle applications.

Acknowledgements

The authors thank the other contributors to this work and particularly B. Vinter, the MBE growth and GaAs processing teams of THALES. The QWIPs R&D at THALES is supported by the French MOD (DGA/STTC/DTCO).

References

- [1] B.F. Levine, J. Appl. Phys. 74 (1993) R1–R81.
- [2] M. Vuillermet, et al., SPIE, San Diego, 1998.
- [3] R. Petit, Electromagnetic Theory of Gratings, in: Topics Current Phys., Vol. 22, Springer, Berlin, 1980.
- [4] J.P. Berenger, J. Comp. Phys. 114 (1994) 185.
- [5] E. Costard, et al., in: Proc. SPIE, Vol. 4130, 2000, pp. 463–472.
- [6] P. Bois, et al., in: Proc. SPIE, Vol. 3061, 1997, pp. 764–771.